Izvestiya Vysshikh Uchebnykh Zavedeniy. Applied Nonlinear Dynamics. 2022;30(5)

Article DOI: 10.18500/0869-6632-003007

Magnetic metasurfaces with metallic inclusions

M. D. Amelchenko[1], *A. S. Bir*[1], *F. Yu. Ogrin*[2,3], *S. A . Odintsov*[1], *D. V. Romanenko*[1], *A. V. Sadovnikov*[1], *S. A. Nikitov*[4], *S. V. Grishin*[1] ✉

[1]Saratov State University, Russia
[2]The University of Exeter, Exeter, England
[3]MaxLLG Ltd., England
[4]Kotelnikov Institute of Radioengineering and Electronics, Moscow, Russia
E-mail: amelchenko.mar@gmail.com, bir.evstegneeva.1997@gmail.com, F.Y.Ogrin@exeter.ac.uk, odinoff@gmail.com, dmitrii.romanenk@mail.ru, sadovnikovav@gmail.com, nikitov@cplire.ru, ✉sergrsh@yandex.ru

Received 1.08.2022, accepted 27.08.2022, published 30.09.2022

Abstract. *Purpose* of this paper is the development and creation of the magnetic metasurfaces with metallic inclusions operating both in the microwave and terahertz frequency ranges. *Methods.* The Maxwell's equations and the expressions for the effective medium parameters are used to build the analytical models of the magnetic metasurfaces based on either a ferromagnetic (FM) or antiferromagnetic (AFM) dielectric matrix, containing a two-dimensional periodic structure of thin metal (non-magnetic) wires surrounded by insulators. Numerical simulation of such structures operating in the microwave range is carried out using the MaxLLG software package. The magnetron sputtering, liquid etching, optical lithography, and lift-off photolithography are used to create bicomponent magnetic metasurfaces, consisting of two magnetic materials with very different values of magnetization. The study of linear and nonlinear characteristics of the bicomponent magnetic metasurfaces is carried out using the methods of microwave and Brillouin spectroscopy. *Results.* Based on the developed analytical model of the magnetic metasurface with metallic (nonmagnetic) inclusions it is shown that the FM metasurface possesses properties of a left-handed medium in a microwave range and the AFM metasurface possesses similar properties in a terahertz range. In the last case, the material parameters of the AFM metasurface are twice negative in two frequency bands. For the magnetic metasurfaces with metallic magnetic inclusions, the formation of absorption bands in the spectrum of a traveling magnetostatic surface spin wave due to the resonant properties of the inclusions has been established. In the nonlinear regime, the effect of nonreciprocal parametric three-wave resonance was obtained. *Conclusion.* The results presented in the paper demonstrate a number of physical phenomena that are observed only in the magnetic metasurfaces with metallic (nonmagnetic and magnetic) inclusions.

Keywords: magnetic metasurfaces, left-handed media, spin waves, parametrical three-wave resonance, nonreciprocity.

Acknowledgements. We would like to aknowledge Ian Wellaway, the software engineer, for technical support in installation and expluatation of MaxLGG software. The work was supported by a grant from the Russian Science Foundation, project № 19-79-20121.

For citation: Amelchenko MD, Bir AS, Ogrin FYu, Odintsov SA, Romanenko DV, Sadovnikov AV, Nikitov SA, Grishin SV. Magnetic metasurfaces with metallic inclusions. Izvestiya VUZ. Applied Nonlinear Dynamics. 2022;30(5):563–590. DOI: 10.18500/0869-6632-003007

Introduction

Metamaterials are artificially created media whose properties differ from natural media. The concept of creating metamaterials is based on the use of periodic structures of subwavelength elements. Their period T is much smaller than the wavelength λ, that is, $T \ll \lambda$. Such elements are created from various materials and their topologies, which are located inside or on the surface of a natural material. With their help, the electric or magnetic response of the medium is artificially modeled. One of the very first theoretically predicted [1, 2] and experimentallyinvestigated [3, 4] metamaterials is the "left" medium [5]. It consists of periodic inclusions in the form of thin metal wires and split ring resonators (SRRs). A periodic structure of thin metal wires simulates a

plasmon medium. Its dielectric properties are described by the effective permittivity. The periodic structure of the SRR models the magnetic properties of the medium. To describe them, an effective magnetic permeability is introduced. Artificially created electric and magnetic responses of the medium change their sign at characteristic frequencies. One of them is determined by the plasma frequency of the plasmonic medium, and the other is determined by the resonant frequency of the SRR. In the left handed medium, the electric and magnetic field intensity vectors together with the wave vector make up the left-handed vector system.The effective permittivity and permeability have negative values. Therefore, left handed medium are often called doubly negative media. In such media, the propagation of the reverse wave is possible. Its phase and group velocity vectors are directed opposite to each other.

Initially, a huge interest in metamaterials was associated with the implementation of the negative refractive index [3] in the left handed medium and the creation of ideal lenses (Pendry lenses) for obtaining images with subwavelength resolution below the Abbe diffraction limit [4]. The adaptation of inhomogeneous and anisotropic refractive index to obtain coatings that create the effect of invisibility ("invisibility cloak"type coatings) pointed to another possibility of using metamaterials for practical purposes. [6]. However, all these potentially promising applications of metamaterials have encountered difficulties. They are associated with strong dispersion and large losses on subwavelength elements in the form of metallic structures. The main problem when creating three-dimensional (3D) metamaterials is the complexity of manufacturing a 3D lattice of micro- and nanoscale subwavelength elements [7]. Planar one-dimensional or two-dimensional (1D or 2D) metamaterials, which are called metasurfaces [8–11], can be created using existing lithography and nanoprinting technologies. As a result, the process of manufacturing metasurfaces is much simpler than in the case of their volumetric analogues.

Since the 2000s, both in our country [12, 13], and abroad [14–18], the concept of magnetic field-controlled double negative media began to develop. They operate in both the microwave and terahertz frequency ranges. Magnets were used for these purposes. They belong to μ-negative media. Their magnetic permeability takes negative values in a certain frequency range, which is in the microwave range in the case of ferromagnets (FM) and in the terahertz range in the case of antiferromagnets (AFM) [19]. Combining their properties with the properties of ε-negative media, which were periodic lattices made of thin wires, made it possible to realize double negative media without using additional subwavelength elements in the form of SRR. For the microwave range, FM materials were used either in the form of films [13, 15] and plates [16] of yttrium iron garnet (YIG), or in the form of ferrite rods [17] or films of BaM ferrites and hexaferrites [18]. Ferrite films LuBiIG [20] and AFM [21] were used for the terahertz range.

Recently, artificial media have also begun to be attributed to metamaterials, in which the period of the structure is comparable to the wavelength, that is, $T \sim \lambda$. In such metamaterials, a wave with a wave number that satisfies the Bragg condition ($k_B = \pi n/T$, where $n = 1, 2, 3...$ — Bragg resonance number), is reflected from the periodic structure and does not pass through the medium. As a result, non-transmission bands are formed at the frequencies of Bragg resonances. They are analogs of the forbidden energy zones that exist in the crystal lattice of any solid. The waves on which it is possible to realize such resonances have a different physical nature. These can be light waves (analogs — quasiparticles photons), and spin waves (analogs — quasiparticles magnons), and sound waves (analogs - quasiparticles phonons). Metamaterials where the Bragg condition is met for light waves are called photonic crystals, for spin waves — magnonic crystals (MC), and for sound waves — phononic crystals [22]. All the crystals listed above can be conditionally attributed to metamaterials of the reflective type.

Films of dielectric ferrite — YIG and metallic ferromagnet — permalloy (Py) are used to create MC. YIG films have a record low ferromagnetic resonance line width (FMR) $\Delta H \leqslant 0.5$ E (relaxation time $\tau_r \geqslant 0.2$ mks) and a relatively small saturation magnetization ($M_0 = 140$ Gs).

Permalloy films are characterized by a significantly larger line width FMR $\Delta H \cong 25...50$ E (relaxation time $\tau_r \geqslant 1...2$ ns) and the saturation magnetization value ($M_0 \cong 796$ Gs) [23]. Due to these features, dipole magnetostatic spin waves (MSW) propagate in the films of the YIG at distances of the order of several millimeters. This is used to create devices for functional processing of analog signals in real time. Permalloy films are of potential interest for the creation of nanometer-sized devices, since MSW in them cover distances of no more than tens of micrometers. Today, 1D and 2D magnetic metasurfaces [24–28], as well as 3D magnonic crystals [29] have been created from these magnetic materials. Their physical properties are investigated using microwave methods and Brillouin spectroscopy methods. Frequency-selective properties of magnetic metasurfaces are of interest for creating various filtering devices based on them. Their reconfigurable properties are used in logic circuits [30]. In addition, there has been a tendency for the MC to move from the microwave to the terahertz range [31].

In addition to metasurfaces that are created from a single magnetic material (single-component magnetic metasurfaces), magnetic metasurfaces in the form of a combination of two magnetic materials (bicomponent magnetic metasurfaces) have been actively studied recently: Co/Py — 1D MC [32–34] and 2D MC [35–39], Py/Fe — 1D MC [40], YIG/Py — 1D and 2D MC [28,41], YIG/Co and YIG/$Co_{20}Fe_{60}B_{20}$ — 2D MC [28], YIG/strips of magnetite nanoparticles — 1D MC [42]. The interest in such artificially created structures is due to the influence of their magnetic properties on the spectrum of the forbidden zones of the MC, as well as the appearance of new properties in bicomponent magnetic metasurfaces that single-component magnetic metasurfaces do not possess. In bicomponent 1D MC, which consist of periodically alternating nanowires with different magnetic properties, the existence of a strong exchange bond at the Co/Py interface was established. It affects the fixing of the dynamic magnetization of [34]. Studies with bicomponent 2D MC have shown that their band structure is much richer compared to 1D MC due to the high density of modes and their subsequent hybridization. The complication of the zone structure here is due to the pronounced inhomogeneity of the internal magnetic field, which occurs due to the effects of static demagnetization [38]. Bicomponent 2D MC are created on the basis of a magnetic "matrix"of one magnetic material and a 2D lattice of another magnetic material, which is embedded in the magnetic matrix in two ways. In the first case, the magnetic matrix contains a 2D lattice of holes in which nanometer-sized magnetic disks are placed [35–39]. In the second case, a 2D grid of square/rectangular magnetic elements of micron size [41] or magnetic nanodiscs [28] is placed directly on the surface of the magnetic matrix. Depending on the properties of the magnetic matrix and the topology of magnetic inclusions in the spectrum of SW traveling in the magnetic matrix, not only Bragg resonances are observed (due to the reflection of SW from the periodic structure), but also absorption frequency bands (due to the resonant properties of the magnetic inclusions themselves) [28, 41]. Absorption is observed for traveling SV with a wavelength that far exceeds the period of the structure ($T \ll \lambda$). The metasurface for such lengths of traveling SV is absorbing.

Magnetic metasurfaces have unique nonlinear properties. They are associated with the development of three- and four-wave nonlinear spin-wave interactions [43]. Four-wave nonlinear spin-wave interactions are caused by the dependence of the amplitude of the vector of macroscopic magnetization on the amplitude of the vector of a high-frequency magnetic field and are used to form envelope solitons at the frequencies of the band gap MC, where there is a strong change in the dispersion of the MSW [44–46]. Three-wave nonlinear spin-wave interactions are caused by the parametric excitation of short-wave exchange SW by a long-wave MSW when the amplitude of the latter reaches a certain threshold value and lead to the simultaneous formation of spatial-temporal chaotic patterns at the frequencies of the decaying wave and the waves parametrically excited by it [47]. Unlike optical systems, where three-wave parametric processes are used to generate the second harmonic (parametric processes with increasing frequency) [48], in magnonics, three-wave

parametric processes are decay processes, that is, processes with decreasing frequency [49]. At the same time, parametrically excited SW can also participate in three-wave fusion processes, as a result of which secondary MSW [50–52] are generated.

Another distinctive feature of parametric three-wave processes in magnonics is their frequency limitation, if the MCV acts as a decaying wave. In this case, the frequency boundaries of parametric three-wave processes depend on the direction and intensity of the external constant magnetic field and the magnetic properties of the material [53]. For magnetic metasurfaces that are made on the basis of films based on yttrium iron garnet bordering free space, parametric three-wave processes are observed at frequencies up to 3.2 GHz if the decaying wave is a volume MSW (VMSW), and at frequencies up to 4.9 GHz if the surface MSW (PMSW) acts as a decaying wave). The influence of the metal, which is located near the surface of the film based on yttrium iron garnet, leads to an expansion of the range of existence of parametric three-wave interactions only for PMSW. In this case, they are observed at frequencies up to 9.8 GHz. The range of existence of parametric three-wave MSW decay processes can also be expanded if permalloy films are used, which have significantly greater magnetization than films based on yttrium iron garnet.

To date, studies of bicomponent magnetic metasurfaces have been carried out in a linear mode. To study the features of parametric three-wave nonlinear spin-wave interaction in such metasurfaces, the case is of interest when two magnetic materials have very different values of magnetization [28, 41]. In such structures, depending on the strength of the external constant magnetic field, parametric excitation of short-wave SW can be carried out simultaneously by MSW in a YIG matrix and standing SW in disks made of metal ferromagnetic and only standing in metal ferromagnetic disks. For metallic ferromagnetic disks, parametric excitation of short-wave SW is expected only at the frequencies of the disks' own resonant modes, which fall into the MSW spectrum and lead to the appearance of absorption bands. If a PMSW is excited in a YIG matrix, which has non-reciprocal properties [54], then in this case an opportunity opens up for studying the phenomenon of non-reciprocal parametric spin-wave resonance in a bicomponent magnetic metasurface.

This paper presents the results of theoretical and experimental studies of linear and nonlinear characteristics of magnetic metasurfaces, which demonstrate unusual properties when wavelength of the traveling wave in a magnetic matrix is greater than the period of metallic (non-magnetic and magnetic) inclusions.

1. Magnetic surface with non-magnetic metal inclusions

Consider a transversely magnetized magnetic metasurface. It consists of a matrix, which is made of magnetically ordered material that is unbounded in all three directions. Its volume contains a 2D periodic structure of thin metallic (non-magnetic) wires with a period of T (Fig. 1). The period of the structure is much smaller than the length of the plane electromagnetic wave (EMW) λ ($T \ll \lambda$), which falls normal to the wires. The external permanent magnetic field $\vec{H}_0$ is directed along the wires. The wave vector $\vec{k}$ is directed perpendicular to the magnetic field $\vec{H}_0$ ($\vec{k} \perp \vec{H}_0$). With this type of magnetization in a magnet, there are EMWS with linear polarization [49]. In this case, the EMW electric field is directed along the axis of the wires. The EMW magnetic field is orthogonal to the electric field. Each wire is surrounded by a layer of non-magnetic dielectric, which isolates the wire from the magnetic matrix to preserve the plasmon properties of the periodic wire structure. For the first time such a metamaterial with the properties of a double negative medium was considered in [55], where the magnetic matrix was made of a ferromagnet. The radius of the wire r_1 was chosen here much smaller than the period

of the structure T. The outer radius of the insulating shell r_2 was chosen from the conditions that $r_2 \cong (r_1 T)^{1/2}$ and $r_1 \ll r_2 \ll T$. In longitudinal magnetization, when the wave vector and the vector of the external constant magnetic field are collinear, the EMW have circular polarization. This is an invalid condition for a double negative environment, which was not taken into account in [56].

It is known [19, 53] that the tensor of the high-frequency magnetic permeability of a magnet that is magnetized along the axis OZ ($\vec{H}_0 \parallel OZ$) is given as

$$\overleftrightarrow{\mu} = \begin{vmatrix} \mu & j\mu_a & 0 \\ -j\mu_a & \mu & 0 \\ 0 & 0 & 1 \end{vmatrix}, \tag{1}$$

where diagonal μ and non-diagonal μ_a tensor components are frequency dependent quantities.

So, for FM

$$\mu = [\omega_H(\omega_H + \omega_M) - \omega^2]/(\omega_H^2 - \omega^2),$$
$$\mu_a = \omega_M \omega/(\omega_H^2 - \omega^2), \tag{2}$$

where $\omega_H = \gamma H_0$ — frequency of FM resonance with longitudinal magnetization, γ — gyromagnetic ratio, $\omega_M = 4\pi\gamma M_0$, $4\pi M_0$ — saturation magnetization of FM. For an AFM with a "light"anisotropy axis coinciding with the OZ axis, the components of the (1) tensor will take the following form [57]:

$$\mu = 1 + 8\pi\gamma_s^2 M_s H_A(\omega_+\omega_- - \omega^2)/[(\omega_+^2 - \omega^2)(\omega_-^2 - \omega^2)],$$
$$\mu_a = 8\pi\gamma_s^2 M_s H_A \omega(\omega_- - \omega_+)/[(\omega_+^2 - \omega^2)(\omega_-^2 - \omega^2)], \tag{3}$$

where γ_s — averaged g-factor; M_s — averaged static magnetization of sublattices; H_A— anisotropy field; $\omega_+ = \gamma_s(H_C + H_0)$, $\omega_- = \gamma_s(H_C - H_0)$ — AFM resonance frequencies; $H_C = [H_A(2H_E + H_A)]^{1/2}$ — the field of "overturning"of sublattices, H_E — the field of homogeneous exchange interaction between sublattices.

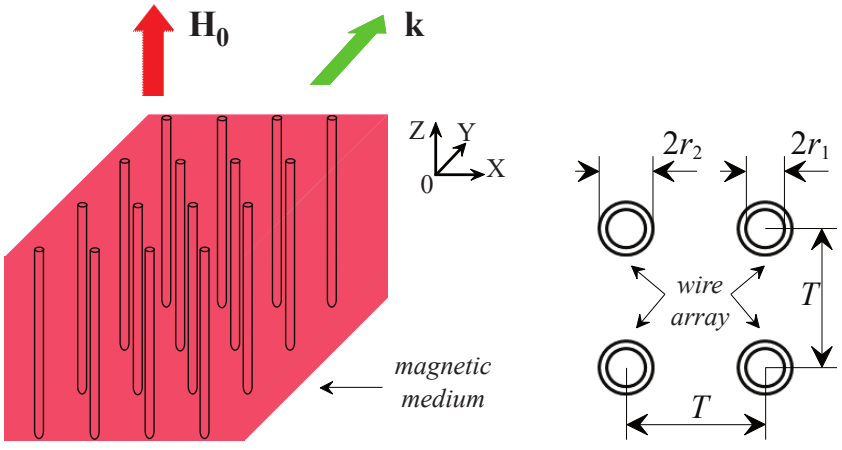

a *b*

Fig. 1. The schemes of (a) a transversely magnetized magnetic metasurface and (b) the 2D periodic array (top view) consisting of the thin wires of a radius r_1 cladded with nonmagnetic insulators of a radius r_2

When solving the electrodynamic problem in the approximation of homogeneous plane waves for TE-EMW that exist in a transversely magnetized unbounded magnetically ordered metamaterial, we obtain the following dispersion equation:

$$k = k_0(\mu_{\text{eff}\perp}\varepsilon_{\text{eff}\perp})^{1/2}, \tag{4}$$

where k is the EMW wave number in the medium, $k_0 = \omega/c$ — the EMW wave number in vacuum, $\omega = 2\pi f$ — circular frequency, f — linear frequency, $\mu_{\text{eff}\perp}$ — effective magnetic permeability of a transversely magnetized magnet, which is determined based on the following expression [19]:

$$\mu_{\text{eff}\perp} = (\mu^2 - \mu_a^2)/\mu, \tag{5}$$

$\varepsilon_{\text{eff}\perp}$ — effective permittivity of a transversely magnetized magnet, which in [14] had the following form:

$$\varepsilon_{\text{eff}\perp} = \varepsilon_r[1 - \omega_{p\perp}^2/(\omega^2 + i\alpha_\perp)], \tag{6}$$

$$\omega_{p\perp}^2 \cong 2\pi/\langle \varepsilon_f T^2 \mu_0 \ln(r_2/r_1) + \mu_{\text{eff}\perp}[\ln(T/r_2) - (3 + \ln 2 - \pi/2)/2]\rangle, \tag{7}$$

$\alpha_\perp = \varepsilon_f \omega \omega_{p\perp}^2/\sigma_{\text{eff}}$, $\varepsilon_f = \varepsilon_0\varepsilon_r$ — absolute permittivity of a magnet, $\varepsilon_0 = 1/(\mu_0 c^2)$ — electrical constant, μ_0 — magnetic constant, ε_r — relative permittivity of the magnet, $\sigma_{\text{eff}} = \pi r_1^2\sigma/T^2$ — effective conductivity of the wire structure, σ — electrical conductivity of the wire. The expression (6) was obtained under the assumption of uniformity of the current density flowing through the wire. This assumption is fulfilled when the radius of the wire is much less than the depth of the skin layer δ, that is, $r_1 \ll \delta = (2/\mu_0\sigma\omega)^{1/2}$ [6].

For a transversely magnetized FM metamaterial, the condition under which $\mu_{ff} < 0$, written as

$$\omega_\perp < \omega < \omega_{ar}, \tag{8}$$

where $\omega_\perp = [\omega_H(\omega_H + \omega_M)]^{1/2}$ — frequency of FM resonance with transverse magnetization, $\omega_{ar} = \omega_H + \omega_M$ — frequency of FM antiresonance.

Conditions under which $\mu_{ff} < 0$, for the AFM metamaterial will be written as

$$\begin{aligned} \omega_{\perp 1} < \omega < \omega_{ar1}, \\ \omega_{\perp 2} < \omega < \omega_{ar2}, \end{aligned} \tag{9}$$

where $\omega_{\perp 1,2} = [\pm(\omega_+ - \omega_-) + D_1^{1/2}]/2$ — two AFM resonance frequencies with transverse magnetization, $\omega_{ar1,2} = [(\omega_+^2 + \omega_-^2 + 8\pi\gamma_s^2 M_s H_A \pm D_2^{1/2})/2]^{1/2}$ — two AFM antiresonance frequencies, $D_1 = (\omega_+ + \omega_-)^2 + 32\pi\gamma_s^2 M_s H_A$, $D_2 = (\omega_+^2 + \omega_-^2 + 8\pi\gamma_s^2 M_s H_A)^2 - 4\omega_+\omega_-(\omega_+\omega_- + 8\pi\gamma_s^2 M_s H_A)$.

In Fig. 2 the frequency dependences of the effective material parameters of the FM and AFM metamaterial are given, calculated on the basis of the relations (5)–(7) taking into account the expressions (2) and (3). From those presented in Fig. 2, *a* of the calculation results, it follows that in the case of an FM metamaterial, there is one frequency band (shown by the fill) in which $\varepsilon_{\text{eff}\perp} < 0$ and $\mu_{\text{eff}\perp} < 0$. This frequency band is in the microwave range. In the case of an AFM metamaterial (Fig. 2, *b*) there are two such areas. They are in the terahertz frequency range. The analytical model of a double negative medium based on a transversely magnetized magnetic material, which contains a periodic structure of thin non-magnetic metal wires surrounded by insulating layers, takes into account only the time dispersion. The model does not take into account the spatial dispersion of the wire structure [58], as well as the reflection of EMW from the periodic structure, as was done in [14].

In Fig. 3 the dispersion characteristics (DC) of TE-EMW, which exist in transversely magnetized FM and AFM media, as well as in metamaterials created on the basis of these media, are given. DC TE-EMW calculations are based on (4). From those presented in Fig. 3, *a*, *c* of the results, it follows that in the absence of a 2D periodic structure ($\omega_{p\perp} = 0$), in the FM

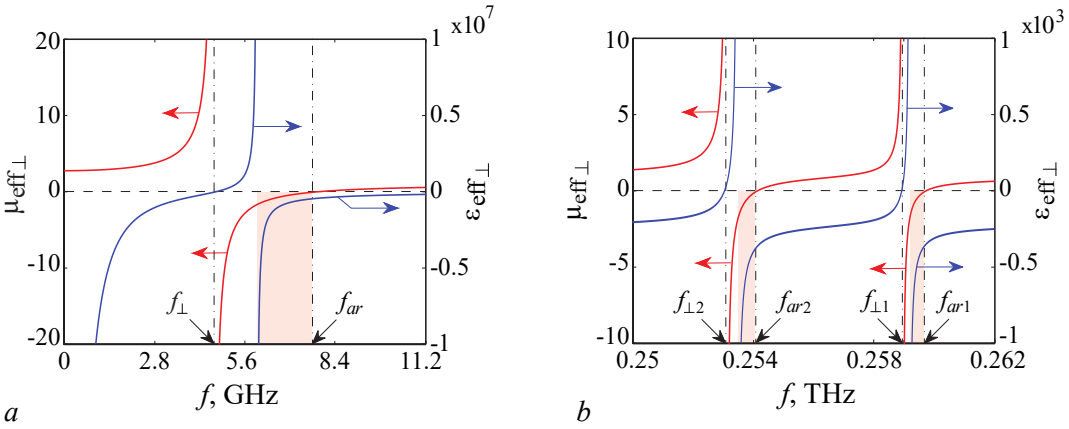

Fig. 2. Effective permeability and permittivity versus frequency f are shown for transversely magnetized FM (a) and AFM (b) metamaterials. The magnetic parameters are used for (a) $M_0 = 139.3$ G and for (b) $H_E = 515$ kOe, $H_A = 8$ kOe, $M_s = 560$ G. For both cases, other parameters are $T = 1.5{\times}10^{-3}$ cm, $r_1 = 10^{-5}$ cm, $r_2 = 1.2{\times}10^{-4}$ cm, $H_0 = 1$ kOe and $\varepsilon_r = 16$

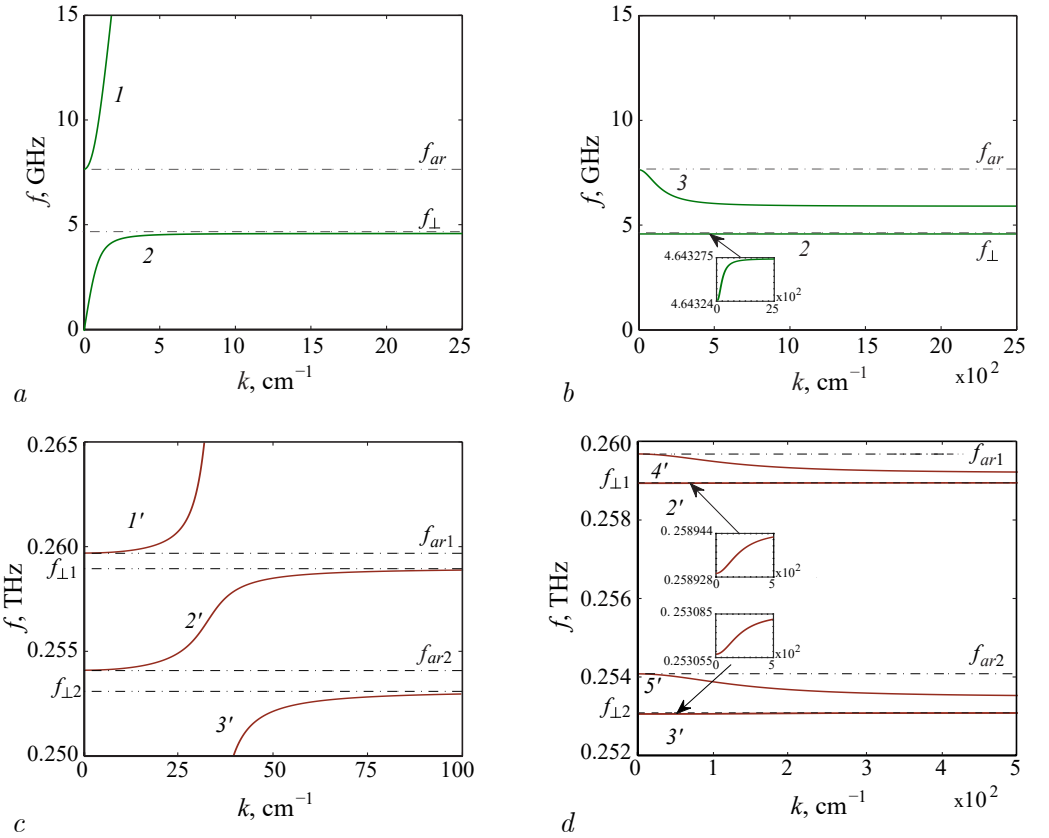

Fig. 3. The dispersion characteristics of extraordinary fast (curves *1* and *1′*) and slow (curves *2*, *3*, and *2′*–*5′*) TE-waves existing in the transversely magnetized FM medium (a) and FM metamaterial (b) as well as AFM media (c) and AFM metamaterial (d). The magnetic parameters used for (a, b) $M_0 = 139.3$ G and for (c, d) $H_E = 515$ kOe, $H_A = 8$ kOe, $M_s = 560$ G. For all cases, other parameters are $T = 1.5 \times 10^{-3}$ cm, $r_1 = 10^{-5}$ cm, $r_2 = 1.2 \times 10^{-4}$ cm, $H_0 = 1$ kOe and $\varepsilon_r = 16$

medium there are two, and in the AFM medium — three unusual TE-EMWs. In the case of an FM medium, one of the two extraordinary TE-EMW is slow, and the other is— fast. In the case of an AFM medium, the number of unusually slow TE-EMWS increases to two. All the listed unusual TE-EMWs are at frequencies where $\mu_{\text{eff}\perp} > 0$ (see Fig. 2). A fast extraordinary TE-EMW has a cut-off frequency, which in the case of an FM medium corresponds to the frequency ω_{ar}, and in the case of an AFM medium — the frequency ω_{ar1}. The slow extraordinary TE-EMW in the FM medium and the low-frequency slow extraordinary TE-EMW in the AFM medium have no cutoff frequency. Their limiting frequencies are the frequencies $\omega_{\perp}$ and $\omega_{\perp 2}$. In a high-frequency slow extraordinary TE-EMW in an AFM medium, the cutoff frequency is the frequency ω_{ar2}, a its limiting frequency is determined by the frequency $\omega_{\perp 1}$. Slow unusual TE-EMWs that exist in transversely magnetized FM and AFM media have only positive (normal) dispersion.

In Fig. 3, *b*, *d* are DC TE-EMW, which are obtained in the presence of a 2D periodic structure of perfectly conducting wires inside the magnet ($\omega_{p\perp} \neq 0$ and $\alpha_{\perp} = 0$). Their radius is less than the depth of the copper skin layer at frequencies of 3 GHz for FM metamaterial and 0.3 THz for AFM metamaterial. In this case, there is a degeneration of forward slow EMW into oscillations at frequencies $\omega_{\perp}$ (for FM metamaterial) and $\omega_{\perp 1,2}$ (for AFM metamaterial), since in the frequency band of the existence of these waves $\mu_{\text{eff}\perp} > 0$, and $\varepsilon_{\text{eff}\perp} < 0$ (see fig. 2). The cutoff frequency of the fast EMW ceases to correspond to the frequency of ω_{ar} (for FM metamaterial) and the frequency of ω_{ar1} (for AFM metamaterial) and shifts to a higher frequency region, where $\mu_{\text{eff}\perp} > 0$ and $\varepsilon_{\text{eff}\perp} > 0$. The most interesting result is the appearance of slow EMWs with negative (anomalous) dispersion, located in the frequency ranges, where $\mu_{\text{eff}\perp} < 0$ and $\varepsilon_{\text{eff}\perp} < 0$ (see fig. 2). In the case of an FM metamaterial, there is one such backward EMW and it is in the microwave range, and in the case of an AFM metamaterial there are two such backward EMWS, and both of them are in the terahertz region. At frequencies where $\mu_{\text{eff}\perp} < 0$, the effective permittivity of the medium can be either less than or greater than zero (see Fig. 2). In this regard, each backward EMW occupies only a part of the frequency range in which $\mu_{\text{eff}\perp} < 0$.

To confirm the existence of backward EMWs in a transversely magnetized magnetic metamaterial, which are predicted by analytical theory, numerical modeling of the FM metamaterial was carried out using the electrodynamic software package MaxLLG [59]. A feature of this package is the joint solution of Maxwell's equations and the equation of motion of the magnetization vector, known as the Landau-Lifshitz-Hilbert equation (LLG), for calculating the characteristics of various magnetic devices. The software package is based on the finite difference method in the time domain. In [60], an algorithm was developed for calculating the discrete LLG equation taking into account anisotropy and exchange fields inside the FDTD grid, which is used in the MaxLLG program.

Initially, a homogeneous FM medium was modeled, for which a model of a transversely magnetized ferromagnet unbounded in all directions was created in the MaxLLG program. The vectors of the external constant magnetic field and magnetization are directed along the $0Z$ axis, and the EMW propagates along the $0Y$ axis. The FM medium is assumed to be homogeneous along the entire length of the EMW propagation. The image of the cross-section of the analyzed structure is shown in Fig. 4, *a*, where the dimensions of the structure are given in pixels (px). The green square with the size of 5×5 px represents a cross-section of the FM medium. The blue area surrounding it is an additional space with vacuum properties, which is designed to absorb possible instabilities arising in the numerical scheme (15 px to the right and left of the green square on the $0X$ axis and 6 px up and down from the green square on the $0Z$ axis). Since an infinite FM medium is considered, periodic boundary conditions were set at the boundaries of the FM medium region in all three directions.

In Fig. 4, *c* shows the results of numerical simulation of DC TE-EMW. Similar dependencies are superimposed on top of them, which are obtained based on the solution of the analytical

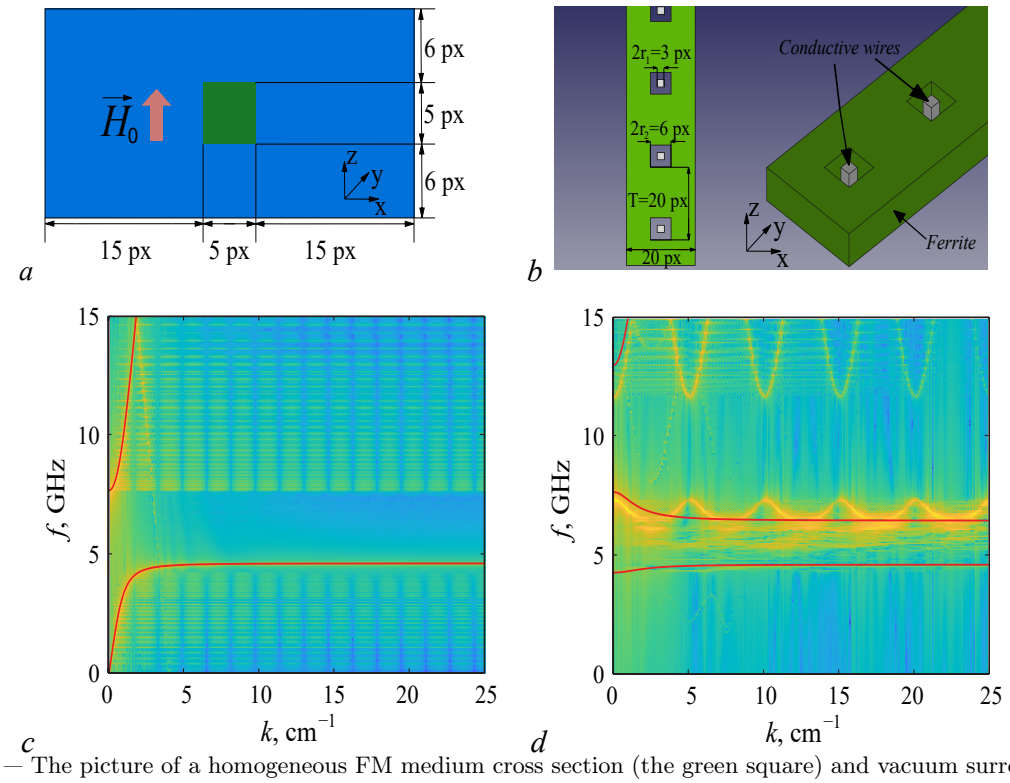

Fig. 4. *a* — The picture of a homogeneous FM medium cross section (the green square) and vacuum surrounding it (the blue area) uploaded to MaxLLG. *b* — The picture of a FM metamaterial model created with FreeCad. *c*, *d* — The dispersion characteristics of fast and slow electromagnetic waves existing in the homogeneous FM medium (*c*) and the FM metamaterial (*d*) that are obtained with the use of MaxLLG (yellow curves) and analytical theory (red curves). The calculation parameter values are $H_0 = 1$ kOe, $M_0 = 139.3$ G, $T = 1.5 \times 10^{-3}$ cm, $r_1 = 10^{-5}$ cm, $r_2 = 1.2 \times 10^{-4}$ cm, $\sigma = 10^8$ S/m and $\varepsilon_r = 16$ (color online)

expression (4) at $\omega_{p\perp} = 0$ for the same parameters of the FM environment. In the numerical experiment, there are also two TE-EMWs with normal dispersion. One of them is fast and the other is slow. For fast TE-EMW, the cutoff frequency corresponds to the frequency f_{ar}. The slow TE-EMW has no cutoff frequency. The limiting frequency is equal to the frequency of the FM resonance $f_\perp$. It is possible to see a complete coincidence between the DC EMW, which are obtained as a result of numerical modeling and by an analytical model, which indicates the correct operation of the MaxLLG software package.

The following are the results of numerical simulation of the FM metamaterial. Its schematic representation is shown in Fig. 4, *b*. When constructing the numerical model, instead of cylindrical holes and wires, square-shaped holes and wires were used. This did not have a noticeable effect on the properties of the plasma structure. The electrical conductivity of the wire was set high enough to reduce losses in them ($\sigma = 10^8$ Cm/m). The elements of the three-dimensional model had the following dimensions: $2r_1 = 3$ px, $2r_2 = 6$ px, $T = 20$ px. A vacuum was used as an insulating layer that separates the wires from the influence of the magnetic fields of the FM medium. The fields in the FM metamaterial were calculated under the same conditions as in a homogeneous FM medium.

In Fig. 4, *d* the results of calculations of the spectra of the TE-EMW FM metamaterial, which are obtained in the MaxLLG software package and based on the solution of the analytical expression (4) at $\omega_{p\perp}, arepresented \neq 0$. It follows from the presented results that a slow reverse wave appears in the EMW spectrum. It is located in the frequency band where the effective material parameters of the medium are twice negative (see Fig. 2). As follows from the predictions of the analytical theory, the backward EMW does not occupy the entire frequency

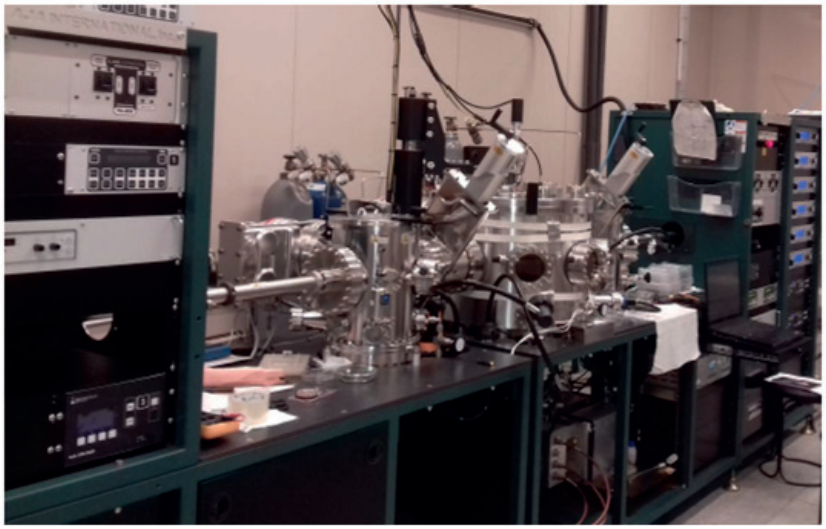

Fig. 5. The external view of the multifunctional ultra-high-vacuum magnetron deposition complex and the magnetron deposition setup

band, where $\mu_{\text{eff}\perp} < 0$, and is limited to the frequency band $\Delta f \approx 1.2$ GHz, where $\mu_{\text{eff}\perp} < 0$ and $\varepsilon_{\text{eff}\perp} < 0$. A low-frequency slow EMW with normal dispersion has a cutoff frequency. The DC of the fast EMW, which is calculated according to the analytical model, is shifted to a higher frequency range. In the case of reverse slow EMW, the discrepancy in the values of cutoff frequencies, which are obtained as a result of numerical modeling and according to analytical theory, does not exceed 4%. The observed discrepancies are due to the fact that when constructing the theoretical model, the influence of the spatial dispersion of the periodic wire structure was not taken into account, as was done, for example, in [58]. Another important result obtained in the framework of numerical modeling in the MaxLLG software package is the presence of periodically repeating regions on the EMW DC. They correspond to Bragg resonances. So, the first Bragg resonance ($n = 1$) here corresponds to the theoretically calculated value of the wave number $k_{\text{B}1}/(2\pi) = 2.5$ cm^{-1}. There are no such resonances on the DC EMW obtained by the analytical model, since the electrodynamic model was built in the approximation of the effective material parameters of the medium.

Thus, the results presented in this section indicate the possibility of creating magnetic metasurfaces based on FM and AFM media with metallic non-magnetic inclusions, which have the properties of double negative media not only in the microwave, but also in the terahertz frequency ranges. A unique feature of AFM-meta surfaces is the simultaneous presence of two frequency ranges in which the material parameters of the medium are twice negative.

2. Magnetic surface with magnetic metal inclusions

This section presents experimental results and results of micromagnetic modeling of linear and nonlinear characteristics of a bicomponent magnetic metasurface, in which metal magnetic inclusions in the form of disks are located on one of the surfaces of a GIG waveguide. The GIG waveguide with a length of 15 mm and a width of 4 mm is made of a GIG film with a thickness of 10 microns and with a saturation magnetization of $M_0 = 139.3$ Gs. The GIG film was grown

by liquid-phase epitaxy on a gallium gadolinium garnet (GGG) substrate with a thickness of 500 microns. A 2D lattice of permalloy disks is formed on the surface of a GIG film with an area of (4×4) mm^2 using magnetron sputtering, liquid etching, optical lithography and explosive (lift-off) photolithography. In the manufacturing process, a multifunctional ultra-high vacuum magnetron deposition complex and a magnetron sputtering unit based on the vacuum post VUP-5M of the Center for Collective Use of the Institute of Microstructure Physics of the Russian Academy of Sciences, Nizhny Novgorod were used (Fig. 5). Lattices of permalloy disks with a diameter of $D = 3weremade...50$ microns, period $T = 6...100$ microns, saturation magnetization $M_0 = 796$ Gs and height $h = 210$ nm, which exceeds the depth of the skin layer. A fragment of one of the manufactured bicomponent magnetic metasurfaces is shown in Fig. 6, *a*.

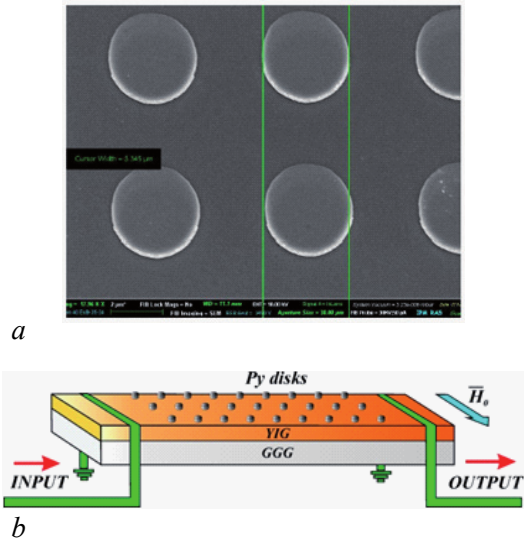

Fig. 6. *a* — The photograph of the bicomponent magnetic metasurface fragment obtained using an electron microscope. *b* — The scheme of the spin-wave transmission line based on the bicomponent magnetic metasurface

Measurements of the module and phase of the transmission coefficient of a bicomponent magnetic metasurface were carried out using a vector analyzer of PNA E8362C circuits. To excite and receive the MSW running in the GIG waveguide, input and output microstrip converters with a width of 50 microns were used, which are grounded at one end, and connected to the generator and load at the other end (Fig. 6, *b*). Microstrip converters of this width are capable of exciting MSW with a minimum wavelength of 100 microns [41], which is comparable to the maximum value of the period T and much greater than its minimum value. A 2D lattice of permalloy disks is located symmetrically between microstrip transducers that are spaced relative to each other by a distance of 7 mm. An external permanent magnetic field H_0 was applied tangentially to the surface of a bicomponent magnetic metasurface and orthogonally to the direction of the MSW propagation. With this configuration of the field, the PMSW propagates in the GIG waveguide.

In Fig. 7 the amplitude-frequency characteristics of a spin-wave transmission line based on a bicomponent magnetic metasurface with maximum values of the diameter of the disks and the lattice period, measured at different field strengths H_0, are given. From the experimental results presented, it follows that several non-transmission bands are observed in the excitation band of the traveling PMSW, which determines the bandwidth of the spin-wave transmission line. They correspond to the PMSW wave numbers, whose values are much smaller than the Bragg wave number $k_{B1} = 314$ rad/cm $(n = 1)$. The appearance of non-transmission bands in the PMSW spectrum occurs according to two scenarios. At relatively small values of the H_0 field, when the bandwidth of the spin-wave transmission line is rebuilt in the frequency range 3...6 GHz (Fig. 7, *a*), one appears at its high-frequency edge first (curve *1*), and then two (curve *2*) non-transmission bands. With an increase in the field strength H_0, they completely disappear, tend to a low-frequency cutoff of the PMSW. At the same time, a third non-transmission band appears near the low-frequency edge of the PMSW bandwidth (curve *3*), which begins to shift up in frequency with an increase in the value of the H_0 field (curves *4* and *5*). At high magnetic field strengths, when the bandwidth of the spin-wave transmission line is rebuilt in the frequency range 6...9 GHz (Fig. 7, *b*), the level of signal suppression in the remaining non-transmission band increases (curves *6* and *7*). From the low-frequency edge, a second (curves *8–12*), and then a

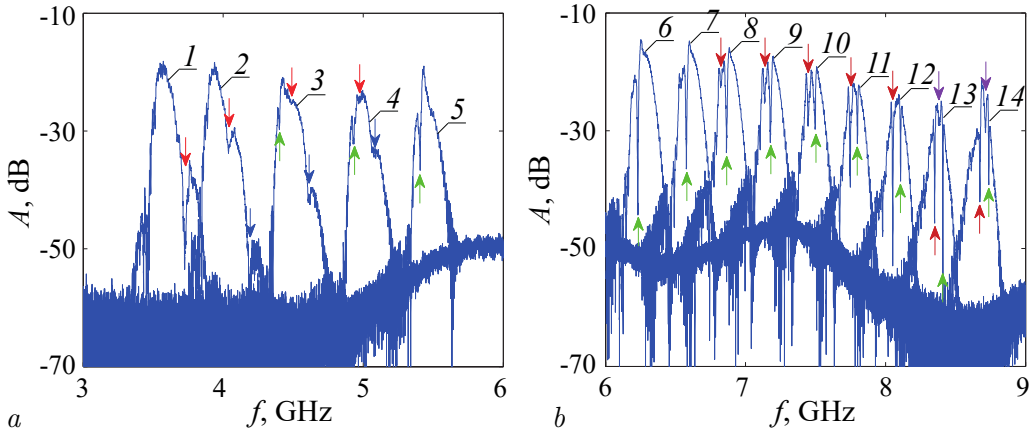

Fig. 7. The AFC of the spin-wave transmission line based on the bicomponent magnetic metasurface with $D = 50$ μm and $T = 100$ μm, demonstrating the stopband control in the frequency range 3...6 GHz (*a*) and 6...9 GHz (*b*) due to a change in the strength field H_0, Oe: 578 (curve *1*), 691 (*2*), 847 (*3*), 1015 (*4*), 1169 (*5*), 1420 (*6*), 1550 (*7*), 1635 (*8*), 1745 (*9*), 1850 (*10*), 1955 (*11*), 2055 (*12*), 2155 (*13*) and 2270 (*14*). In (*a*), the red and blue arrows show the stopbands, the transformation of which occurs according to the first scenario. In (*a*), (*b*), the green, maroon and purple arrows show the stopbands, the transformation of which occurs according to the second scenario (color online)

third (curves *13* and *14*) non-transmission bands appear from it. Unlike the first scenario, when the non-transmission bands shift to the low-frequency edge of the PMSW band and completely disappear with an increase in the value of the H_0 field, according to the second scenario, the non-transmission bands shift towards the high-frequency edge of the PMSW band and do not disappear with an increase in the field to $H_0 = 2270$ E. Reducing the period of the structure from 100 microns to 6 microns and the diameter of the disks from 50 microns to 3 microns leads to the disappearance of the first scenario. Here, only low-frequency non-transmission bands are observed, which shift towards the high-frequency cutoff of the PMSW band with an increase in the magnetic field strength. The non-transmission bands observed by us in the experiment are absorption bands that arise as a result of excitation of one of the resonant types of vibrations of permalloy resonators by means of a PMSW running in a GIG waveguide. In [41], the absorption bands were well identified only when the orthogonality between the wave vector of the PMSW and the vector of the external constant magnetic field was violated.

The dispersion characteristics of the PMSW propagating in a GIG waveguide with a 2D permalloy disk lattice were calculated from the measured phase frequency characteristics in the same way as it was done in [41]. In Fig. 8 the dependences of the PMSW wave numbers, which correspond to the central frequencies of the non-transmission bands, on the magnitude of the internal magnetic field $H_\text{i} = H_0 + H_\text{a}$ (where H_a is the anisotropy field) are given. In all cases, the wave number of the PMSW is less than $k_{\text{B}1}$ and depends almost linearly on the magnitude of the field H_i. This proves that the non-transmission bands observed in the experiment are formed at the PMSW lengths, which significantly exceed the Bragg wavelength and are not the result of reflection of the traveling PMSW from the periodic structure.

To confirm the mechanism of the formation of non-transmission bands due to the ingress of one of the permalloy disk's own modes into the PMSW band running in a YIG waveguide, micromagnetic modeling of the frequency characteristics of a single permalloy disk and a GIG waveguide was carried out using the MuMax3 software package. The simulation used a modification of the finite element method [61], which consisted in solving the Landau-Lifshitz-Hilbert equation method Dorman–Prince [62]. When simulating the PMSW in a GIG waveguide, regions with exponentially increasing attenuation coefficient were introduced at the edges of the system to reduce signal reflections from the boundaries of the computational domain.

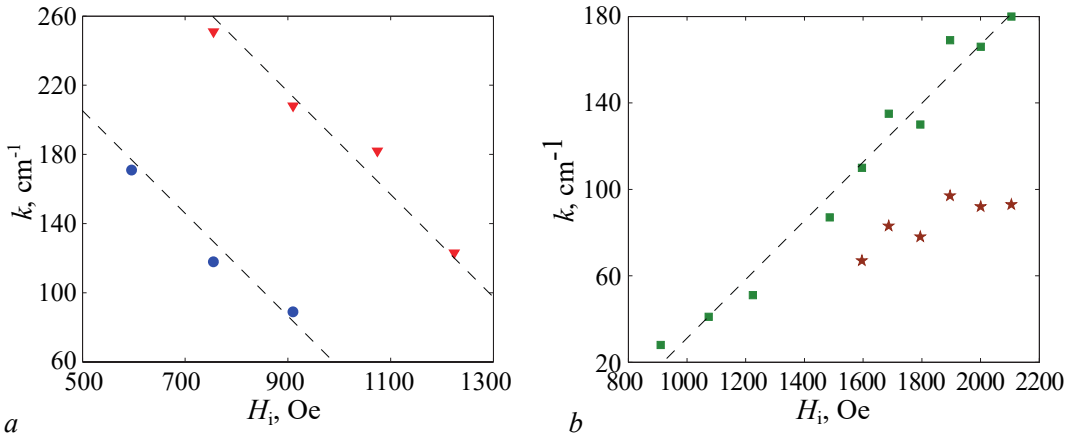

Fig. 8. The dependences of the MSSW wave numbers k, corresponding to the central frequencies of two high-frequency (a) and two low-frequency (b) stopbands of the bicomponent magnetic metasurface, on the internal magnetic field value H_i

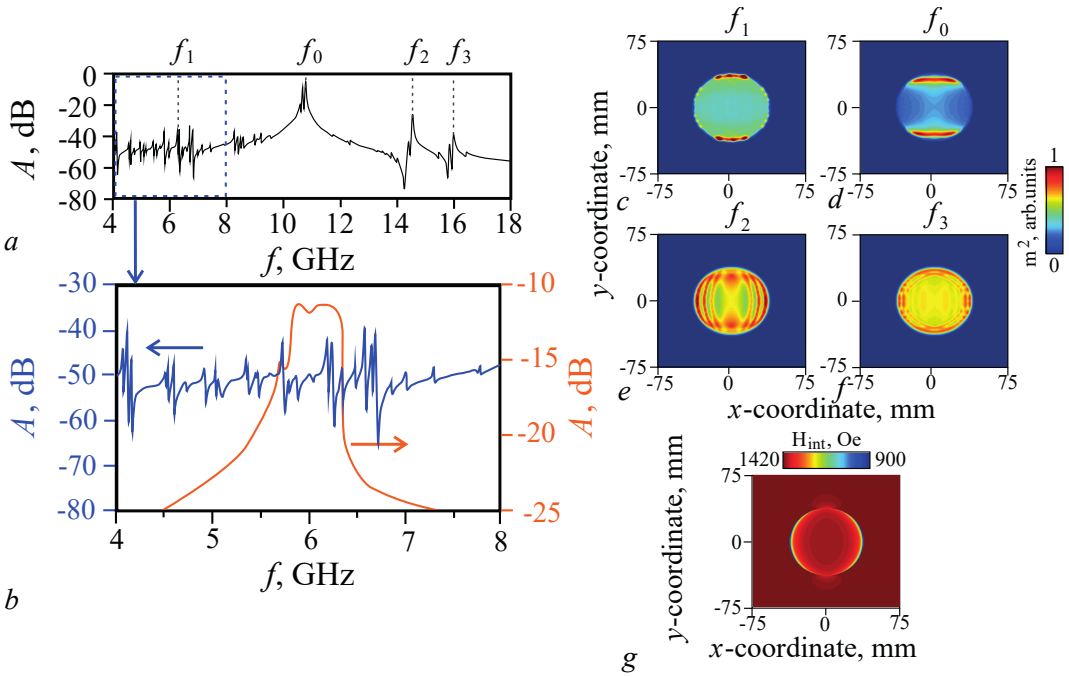

Fig. 9. The AFC of a permalloy disk with $D = 50$ μm, $h = 200$ nm and $M_0 = 796$ G, located in the external static magnetic field $H_0 = 1420$ Oe, (a) and its comparison with a YIG waveguide AFC (orange curve), the parameters of which are also taken from the experiment (b); the distribution maps of the magnetization amplitude square m^2 simulated at frequencies $f_1 = 6.325$ GHz (c), $f_0 = 10.7$ GHz (d), $f_2 = 14.55$ GHz (e), and $f_3 = 16.0$ GHz (f) for a permalloy disk; the internal magnetic field distribution of the permalloy disk (g) (color online)

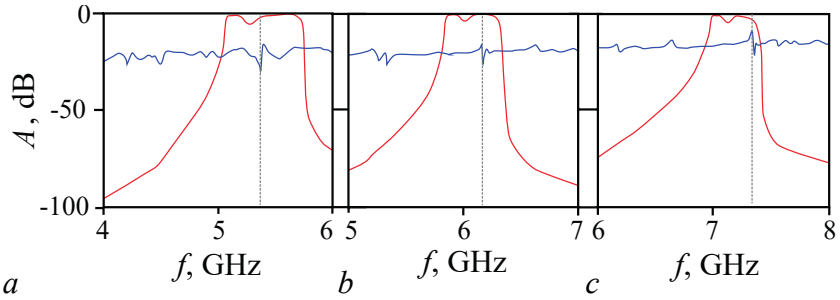

Fig. 10. The AFCs of a permalloy disk with $D = 3$ μm (blue curve) and a YIG waveguide (red curve) calculated for several values of the external static magnetic field H_0: 847 Oe (a), 1420 Oe (b) and 1745 Oe (c). In all AFCs, the dotted line shows the frequency of one of the eigenmodes of the permalloy disk

In Fig. 9 the frequency spectrum of the eigenmodes of the Permalloy disk is given. From those presented in Fig. 9, a of the results it follows that the permalloy disk is a magnetic resonator, the frequency f_0 of the main (fundamental) type of oscillation of which, unlike a traditional (non-magnetic) resonator, is not the smallest. With transverse magnetization, it is near the frequency $f_\perp = \sqrt{f_H(f_H + f_M)} = 11.275$ GHz. The frequencies of the subsequent types of oscillations (see Fig. 9, a, c–f) can be located higher in frequency (fall on the frequency spectrum of the PMSW for permalloy) and lower in frequency (fall on the frequency spectrum of the OOMSW for permalloy). This feature of the magnetic resonator is due to the presence of a highly inhomogeneous internal magnetic field (see Fig. 9, g). Its distribution and magnitude can be controlled by changing the diameter of the resonator and the intensity of the external permanent magnetic field. The frequency arrangement of the PMSW spectrum propagating in the GIG waveguide also depends on the magnitude of the latter (see Fig. 9, b). By selecting the magnetic parameters of the system, it is possible to achieve a situation where some of the intrinsic modes of the magnetic resonator will fall into the spectrum of the traveling PMSW. As follows from the results presented in Fig. 9, b, at $H_0 = 1420$ E, at least one of the eigenmodes of the permalloy resonator falls into the PMSW band, the excitation of which by the surface MSW leads to the absorption of the latter's energy and to the formation of a non-transmission band at a given frequency. In the experiment, at the same field value, only one non-transmission band is observed in the PMSW spectrum (see Fig. 7, b — curve *6*).

The results of modeling the amplitude-frequency characteristics of a GIG waveguide and a single permalloy disk with a change in the field strength H_0 are shown in Fig. 10. It can be seen that as the magnetic field strength increases, the frequency spectra of the permalloy disk and the GIG waveguide shift up in frequency. However, the resonant frequency of one of the eigenmodes of the permalloy disk is shifted more strongly than the PMSW band. This corresponds to the second scenario of the non-transmission band behavior, which is observed in the experiment at these frequencies.

In addition to controlling the absorption bands of bicomponent magnetic metasurfaces, which is carried out in a linear mode by changing the field strength H_0, experimental studies of the amplitude characteristics of metasurfaces in a nonlinear mode were carried out. The studies were carried out at frequencies where three-wave nonlinear spin-wave interactions were allowed for the GIG waveguide and for permalloy disks, and at frequencies where three-wave nonlinear spin-wave interactions were prohibited for PMCs running in the GIG waveguide (only four-wave nonlinear spin-wave interactions are allowed), but allowed for standing modes OOMSW in permalloy disks. For the first case, frequencies below 4 GHz were selected, and for the second case — slightly above 5 GHz. The results obtained for two cases are shown in Fig. 11. From those presented in

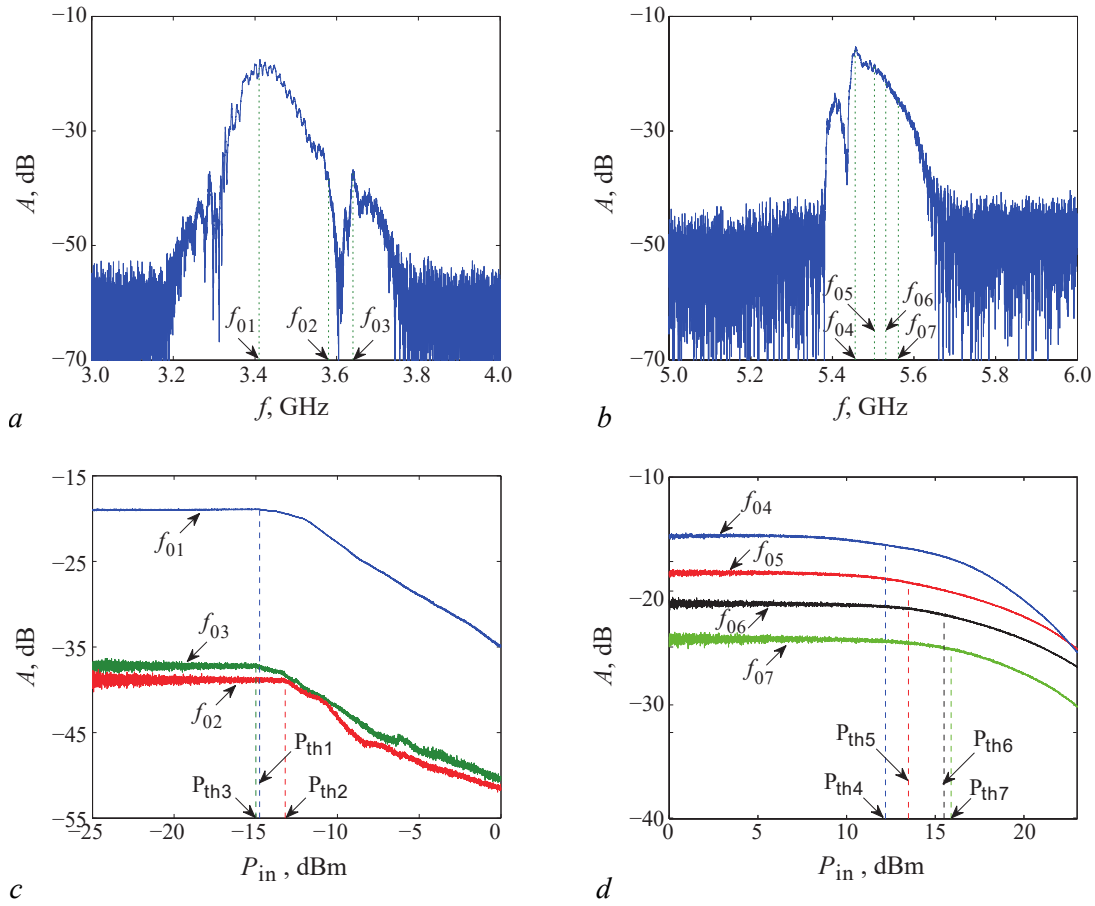

Fig. 11. The AFCs (*a*, *b*) and power characteristics (*c*, *d*) of the spin-wave transmission line based on the bicomponent magnetic metasurface, measured at two values of the field H_0: 530 Oe (*a*, *c*) and 1190 Oe (*b*, *d*). The measurements were carried out for the metasurface with the diameter and period of the permalloy disks $D = 50$ μm and $T = 100$ μm (color online)

Fig. 11, *a*, *c* of the results it follows that the creation of a 2D structure of permalloy disks on the surface of the film leads to a significant change in the threshold levels of incident power, at which three-wave nonlinear processes of decay of the PMSW running in the GIG-waveguide. For a spin-wave transmission line based on a homogeneous GIG film, the threshold levels of incident power measured at different PMSW frequencies are minimal and correspond to the values of $-21... - 19$ dBm. They increase with an increase in the density of the placement of magnetic disks on a given area of the YIG waveguide to the values of $-15... - 13$ dBm (see fig. 11, *c*). As follows from the results presented in Fig. 11, *b*, *d*, if only four-wave nonlinear spin-wave interactions are realized in the GIG waveguide, then the incident power levels (measured by the level of deviation of 1 dB from the linear case), at which these interactions develop and have much larger values $(+12... + 16$ dBm) than in the case of three-wave interactions.

The study of the spectra and spatial distribution of the intensity of spin-wave excitations at the fundamental frequency (the frequency of the PMSW traveling in a GIG waveguide) and at half the frequencies (the frequencies of parametrically excited SW) was carried out using the Mandelstam– Brillouin scattering of light (MBRS, MBLS). This installation consists of a six-pass Fabry-Pero interferometer–Scientific Instruments TFP-I pen and Excelsior-532 Spectra-Physics single-mode solid-state laser with a wavelength of 532 nm and a generation line width of 8 MHz. The use of this installation makes it possible to obtain information about the local dynamics of magnetization due to a focused laser spot with a diameter of 25 microns on the surface of

the sample. The dynamics of magnetization was studied in the geometry of quasi-inverse light scattering at room temperature 295 K. To fulfill the requirement that there is no thermal change in the properties of the measured sample, the laser radiation power supplied to the sample was 1 MW per spot. The scattered light was studied at different values of the distance between the mirrors of the tandem circuit.

In Fig. 12 the amplitude-frequency characteristic of a spin-wave transmission line based on a bicomponent magnetic metasurface, measured using a circuit analyzer in the frequency domain, is given. At the same time, three-wave parametric spin-wave interactions are prohibited for a PMSW running in a GIG waveguide. In linear mode, there are two absorption bands in the PMSW spectrum with central frequencies $f_{p2} = 6.224$ GHz and $f_{p4} = 6.258$ GHz. Changing the direction of the magnetic field to the opposite ($H_0 = -1400$ E) leads to a change not only in the level of signal attenuation, but also in the frequency arrangement of the absorption bands in the PMSW spectrum. Now only one absorption band with a central frequency of $f_{p3} = 6.243$ GHz is observed in the PMSW spectrum.

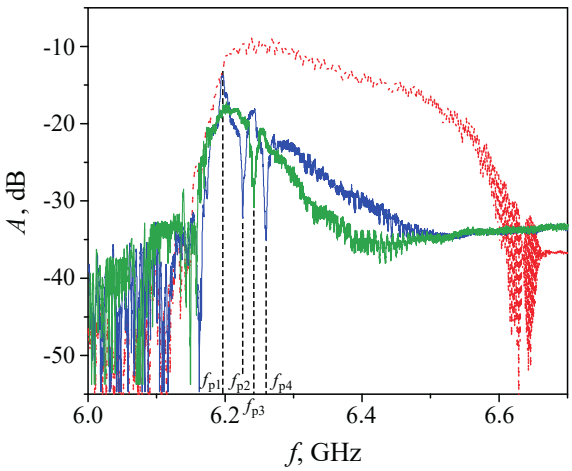

Fig. 12. The AFCs of the spin-wave transmission line based on the bicomponent magnetic metasurface with the 2D lattice of the permalloy disks with $D = 50$ μm and $T = 100$ μm, measured in the linear mode for the strength of the external static magnetic field $H_0 = 1400$ Oe (blue curve) and $H_0 = -1400$ Oe (green curve). The AFC of the spin-wave transmission line based on the homogeneous YIG film is marked by the red dotted line. The dotted lines show the frequencies for the MBLS experiment (color online)

The explanation for this is as follows. In the opposite direction of the H_0 field, the PMSW begins to propagate efficiently along the opposite surface of the GIG waveguide, which does not border on the Permalloy disk lattice. As a result, there is a change in the dispersion of the PMSW and the internal magnetic field both in the GIG waveguide itself and in permalloy disks in contact with its surface. In this case, the proper modes of permalloy disks begin to correspond to other wave numbers of the PMSW running in the YIG waveguide, .Therefore, absorption bands will be observed at other frequencies. The spectrum of PMSW in two directions of the magnetic field is at frequencies above 4.9 MHz, where three-wave decay processes are prohibited for PMSW propagating in a free GIG film [53]. However, for permalloy, three-wave decay processes of standing OOMSW will be allowed, since these processes are observed at frequencies up to 18.7 GHz.

The parametric excitation of the SW was studied for the PMSW frequencies located outside the absorption bands and at their central frequencies. From those presented in Fig. 13 of the results it follows that at $H_0 = 1400$ E parametric excitation of SW is observed at frequencies $f_{p2}/2$ and $f_{p4}/2$, when the frequencies of PMSW are f_{p2} and f_{p4} correspond to the central frequencies of the absorption bands at which the parametric excitation of the SW is carried out by one of the eigenmodes of vibrations of the small disks. There is no parametric excitation of SW at frequencies f_{p1} and f_{p3} located outside the specified absorption bands at frequencies $f_{p1}/2$ and $f_{p3}/2$.

Changing the frequencies of the proper modes of Permalloy disks when changing the direction of the external constant magnetic field to the opposite leads to a change in the conditions of parametric resonance. At the frequencies f_{p2} and f_{p4}, at which, at the field $H_0 = 1400$ E, there

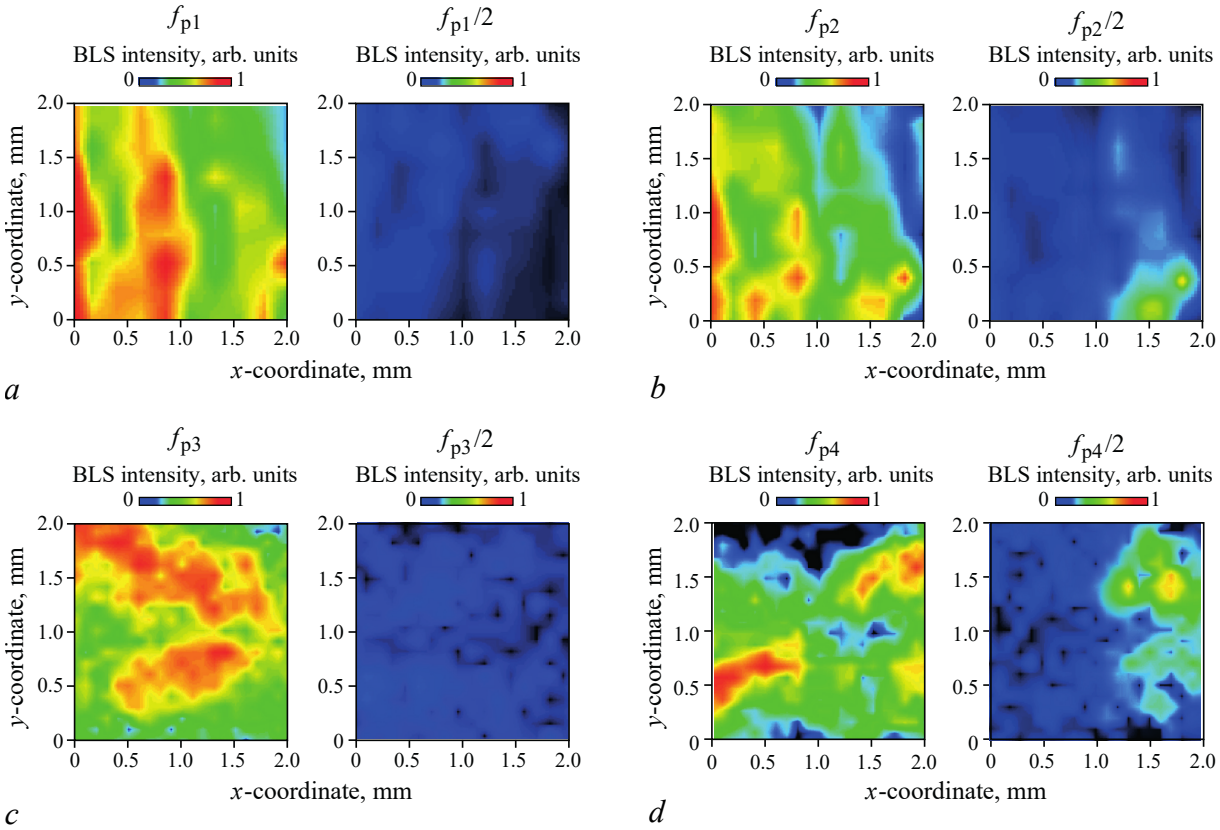

Fig. 13. The spatial distributions of the MSSW magnetization (left panels in (a–d)) and parametrically excited SWs (right panels in (a–d)) of the bicomponent magnetic metasurface with the 2D lattice of the permalloy disks with $D = 50$ μm and $T = 100$ μm, measured using the MBLS setup. The distributions were obtained for the strength of the external static magnetic field $H_0 = 1400$ Oe and the following MSSW and SW frequencies: $f_{p1} = 6.193$ GHz and $f_{p1}/2$ (a), $f_{p2} = 6.224$ GHz and $f_{p2}/2$ (b), $f_{p3} = 6.243$ GHz and $f_{p3}/2$ (c), $f_{p4} = 6.258$ GHz and $f_{p4}/2$ (d). At all MSSW frequencies, the signal power at the input of the spin-wave transmission line is +30 dBm

were absorption bands and there was a parametric resonance for standing OOMSW in permalloy disks, at the field $H_0 = -1400$ E, there are no absorption bands at these frequencies. Parametric three-wave resonance is prohibited for a PMSW running in a GIG waveguide. As follows from the results presented in Fig. 12, fig. 13 and fig. 14, at the frequency f_{p3}, at which with the field $H_0 = 1400$ E there was no absorption band and parametric resonance conditions for the PMSW in the GIG waveguide, with a field $H_0 = -1400$ E at the specified frequency there is an absorption band in which the conditions of parametric resonance for standing OOMSW in permalloy disks are fulfilled. As a result, we observe a new effect — the effect of *non-reciprocal parametric three-wave resonance*, which is characteristic only of a bicomponent magnetic metasurface consisting of magnetic materials with strongly different magnetization.

Conclusion

The results presented in this paper demonstrate a number of physical phenomena (the simultaneous existence of two frequency regions in which the material parameters of the medium are twice negative, and non-reciprocal parametric three-wave resonance), which are observed only in magnetic metasurfaces with metallic (non-magnetic and magnetic) inclusions. In the future, the development and creation of functional devices for processing and storing information signals based on active magnetic metasurfaces for the microwave and terahertz frequency ranges is of

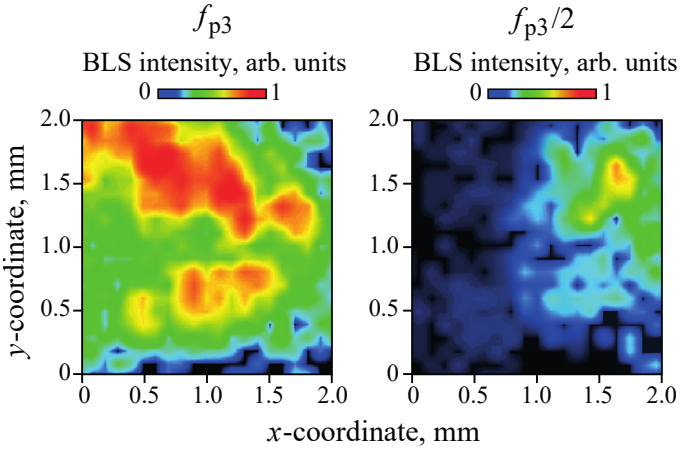

Fig. 14. The spatial distributions of the MSSW magnetization (left panel) and parametrically excited SWs (right panel) of the bicomponent magnetic metasurface with the 2D lattice of the permalloy disks with $D = 50$ μm and $T = 100$ μm, measured using the MBLS setup. The distributions were obtained for the strength of the external static magnetic field $H_0 = -1400$ Oe at the MSSW frequency $f_{p3} = 6.243$ GHz and SW frequency $f_{p3}/2$. At the MSSW frequency, the signal power at the input of the spin-wave transmission line is +30 dBm

interest.

References

1. Veselago VG. Electrodynamics of substances with simultaneously negative values ε and μ. Sov. Phys. Usp. 1968;10(4):509–514. DOI: 10.1070/PU1968v010n04ABEH003699.
2. Pendry JB, Holden AJ, Stewart WJ, Youngs I. Extremely low frequency plasmons in metallic mesostructures. Phys. Rev. Lett. 1996;76(25):4773–4776. DOI: 10.1103/PhysRevLett.76.4773.
3. Smith DR, Padilla WJ, Vier DC, Nemat-Nasser SC, Schultz S. Composite medium with simultaneously negative permeability and permittivity. Phys. Rev. Lett. 2000;84(18):4184–4187. DOI: 10.1103/PhysRevLett.84.4184.
4. Pendry JB. Negative refraction makes a perfect lens. Phys. Rev. Lett. 2000;85(18):3966–3969. DOI: 10.1103/PhysRevLett.85.3966.
5. Sharaevsky YP. Left-handed media: what is interesting? Izvestiya VUZ. Applied Nonlinear Dynamics. 2012;20(1):33–42 (in Russian). DOI: 10.18500/0869-6632-2012-20-1-33-42.
6. Schurig D, Mock JJ, Justice BJ, Cummer SA, Pendry JB, Starr AF, Smith DR. Metamaterial electromagnetic cloak at microwave frequencies. Science. 2006;314(5801):977–980. DOI: 10.1126/science.1133628.
7. Soukoulis CM, Wegener M. Past achievements and future challenges in the development of three-dimensional photonic metamaterials. Nature Photonics. 2011;5(9):523–530. DOI: 10.1038/nphoton.2011.154.
8. Kildishev AV, Boltasseva A, Shalaev VM. Planar photonics with metasurfaces. Science. 2013;339(6125):1232009. DOI: 10.1126/science.1232009.
9. Glybovski SB, Tretyakov SA, Belov PA, Kivshar YS, Simovski CR. Metasurfaces: From microwaves to visible. Physics Reports. 2016;634:1–72. DOI: 10.1016/j.physrep.2016.04.004.
10. Chen HT, Taylor AJ, Yu N. A review of metasurfaces: physics and applications. Rep. Prog. Phys. 2016;79(7):076401. DOI: 10.1088/0034-4885/79/7/076401.
11. Remnev MA, Klimov VV. Metasurfaces: a new look at Maxwell's equations and new ways to control light. Phys. Usp. 2018;61(2):157–190. DOI: 10.3367/UFNe.2017.08.038192.
12. Bespyatykh YI, Bugaev AS, Dikshtein IE. Surface polaritons in composite media with time dispersion of permittivity and permeability. Physics of the Solid State. 2001;43(11):2130–

2135. DOI: 10.1134/1.1417193.
13. Vashkovskii AV, Lokk EH. Negative refractive index for a surface magnetostatic wave propagating through the boundary between a ferrite and ferrite-insulator-metal media. Phys. Usp. 2004;47(6):601–605. DOI: 10.1070/PU2004v047n06ABEH001793.
14. Dewar G. Minimization of losses in a structure having a negative index of refraction. New J. Phys. 2005;7:161. DOI: 10.1088/1367-2630/7/1/161.
15. He Y, He P, Yoon SD, Parimi PV, Rachford FJ, Harris VG, Vittoria C. Tunable negative index metamaterial using yttrium iron garnet. J. Magn. Magn. Mater. 2007;313(1):187–191. DOI: 10.1016/j.jmmm.2006.12.031.
16. Zhao H, Zhou J, Zhao Q, Li B, Kang L, Bai Y. Magnetotunable left-handed material consisting of yttrium iron garnet slab and metallic wires. Appl. Phys. Lett. 2007;91(13):131107. DOI: 10.1063/1.2790500.
17. Bi K, Zhou J, Zhao H, Liu X, Lan C. Tunable dual-band negative refractive index in ferrite-based metamaterials. Opt. Express. 2013;21(9):10746–10752. DOI: 10.1364/OE.21.010746.
18. Rachford FJ, Armstead DN, Harris VG, Vittoria C. Simulations of ferrite-dielectric-wire composite negative index materials. Phys. Rev. Lett. 2007;99(5):057202. DOI: 10.1103/PhysRevLett.99.057202.
19. Gurevich AG. Ferrite in Microwaves. Moscow: Fizmatgiz; 1960. 407 p. (in Russian).
20. Huang YJ, Wen GJ, Li TQ, Li JLW, Xie K. Design and characterization of tunable terahertz metamaterials with broad bandwidth and low loss. IEEE AWP Letters. 2012;11:264–267.DOI: 10.1109/LAWP.2012.2189090.
21. Grishin SV, Amel'chenko MD, Sharaevskii YP, Nikitov SA. Double negative media based on antiferromagnetic metamaterials Tech. Phys. Lett. 2021;47(18):32–35 (in Russian). DOI: 10.21883/PJTF.2021.18.51470.18873.
22. Evtikhov MG, Nikitov SA. Semigroup method for calculation of the spectra of photonic, phononic, and magnonic crystals. J. Commun. Technol. Electron. 2008;53(3):241–255. DOI: 10.1134/S1064226908030017.
23. Melkov GA, Koblyanskiy YV, Slipets RA, Talalaevskij AV, Slavin AN. Nonlinear interactions of spin waves with parametric pumping in permalloy metal films. Phys. Rev. B. 2009;79(13):134411. DOI: 10.1103/PhysRevB.79.134411.
24. Nikitov SA, Tailhades P, Tsai CS. Spin waves in periodic magnetic structures–magnonic crystals. J. Magn. Magn. Mater. 2001;236(3):320–330. DOI: 10.1016/S0304-8853(01)00470-X.
25. Kruglyak VV, Demokritov SO, Grundler D. Magnonics. J. Phys. D: Appl. Phys. 2010;43(26):264001. DOI: 10.1088/0022-3727/43/26/264001.
26. Serga AA, Chumak AV, Hillebrands B. YIG magnonics. J. Phys. D: Appl. Phys. 2010;43(26):264002. DOI: 10.1088/0022-3727/43/26/264002.
27. Gubbiotti G, Tacchi S, Madami M, Carlotti G, Adeyeye AO, Kostylev M. Brillouin light scattering studies of planar metallic magnonic crystals. J. Phys. D: Appl. Phys. 2010;43(26):264003. DOI: 10.1088/0022-3727/43/26/264003.
28. Yu H, Chen J, Cros V, Bortolotti P, Wang H, Guo C, Brandl F, Heimbach F, Han X, Anane A, Grundler D. Active ferromagnetic metasurface with topologically protected spin texture for spectral filters. Adv. Funct. Mater. 2022;32(34):2203466. DOI: 10.1002/adfm.202203466.
29. Popov PA, Sharaevskaya AY, Beginin EN, Sadovnikov AV, Stognij AI, Kalyabin DV, Nikitov SA. Spin wave propagation in three-dimensional magnonic crystals and coupled structures. J. Magn. Magn. Mater. 2019;476:423–427. DOI: 10.1016/j.jmmm.2018.12.008.
30. Khitun A, Bao M, Wang KL. Magnonic logic circuits. J. Phys. D: Appl. Phys. 2010;43(26):264005. DOI: 10.1088/0022-3727/43/26/264005.

31. Zakeri K. Magnonic crystals: towards terahertz frequencies. J. Phys. Condens. Matter. 2020;32(36):363001. DOI: 10.1088/1361-648X/ab88f2.
32. Wang ZK, Zhang VL, Lim HS, Ng SC, Kuok MH, Jain S, Adeyeye AO. Observation of frequency band gaps in a one-dimensional nanostructured magnonic crystal. Appl. Phys. Lett. 2009;94(8):083112. DOI: 10.1063/1.3089839.
33. Sokolovskyy ML, Krawczyk M. The magnetostatic modes in planar one-dimensional magnonic crystals with nanoscale sizes. J. Nanopart. Res. 2011;13(11):6085–6091. DOI: 10.1007/s11051-011-0303-5.
34. Zhang VL, Lim HS, Lin CS, Wang ZK, Ng SC, Kuok MH, Jain S, Adeyeye AO, Cottam MG. Ferromagnetic and antiferromagnetic spin-wave dispersions in a dipole-exchange coupled bicomponent magnonic crystal. Appl. Phys. Lett. 2011;99(14):143118. DOI: 10.1063/1.3647952.
35. Duerr G, Madami M, Neusser S, Tacchi S, Gubbiotti G, Carlotti G, Grundler D. Spatial control of spin-wave modes in Ni80Fe20 antidot lattices by embedded Co nanodisks. Appl. Phys. Lett. 2011;99(20):202502. DOI: 10.1063/1.3662841.
36. Tacchi S, Duerr G, Klos JW, Madami M, Neusser S, Gubbiotti G, Carlotti G, Krawczyk M, Grundler D. Forbidden band gaps in the spin-wave spectrum of a two-dimensional bicomponent magnonic crystal. Phys. Rev. Lett. 2012;109(13):137202. DOI: 10.1103/PhysRevLett.109.137202.
37. Gubbiotti G, Tacchi S, Madami M, Carlotti G, Jain S, Adeyeye AO, Kostylev MP. Collective spin waves in a bicomponent two-dimensional magnonic crystal. Appl. Phys. Lett. 2012;100(16):162407. DOI: 10.1063/1.4704659.
38. Zivieri R. Bandgaps and demagnetizing effects in a Py/Co magnonic crystal. IEEE Trans. Magn. 2014;50(11):1100304. DOI: 10.1109/TMAG.2014.2324174.
39. Malagó P, Giovannini L, Zivieri R, Gruszecki P, Krawczyk M. Spin-wave dynamics in permalloy/ cobalt magnonic crystals in the presence of a nonmagnetic spacer. Phys. Rev. B. 2015;92(6):064416. DOI: 10.1103/PhysRevB.92.064416.
40. Gubbiotti G, Tacchi S, Madami M, Carlotti G, Yang Z, Ding J, Adeyeye AO, Kostylev M. Collective spin excitations in bicomponent magnonic crystals consisting of bilayer permalloy/Fe nanowires. Phys. Rev. B. 2016;93(18):184411. DOI: 10.1103/PhysRevB.93.184411.
41. Vysotskii SL, Khivintsev YV, Sakharov VK, Novitskii NN, Dudko GM, Stognii AI, Filimonov YA. Surface magnetostatic waves in yttrium–iron garnet with the surface subwave metastructure of a permalloy film. Physics of the Solid State. 2020;62(9):1659–1663. DOI: 10.1134/S1063783420090334.
42. Lazcano-Ortiz Z, Ordóñez-Romero CL, Domínguez-Juárez JL, Monsivais G, Quintero-Torres R, Matatagui D, Fragoso-Mora JR, Qureshi N, Kolokoltsev O. Magnonic crystal with strips of magnetic nanoparticles: Modeling and experimental realization via a dip-coating technique. Magnetochemistry. 2021;7(12):155. DOI: 10.3390/magnetochemistry7120155.
43. L'vov VS. Nonlinear Spin Waves. Moscow: Nauka; 1987. 272 p. (in Russian).
44. Ustinov AB, Grigor'eva NY, Kalinikos BA. Observation of spin-wave envelope solitons in periodic magnetic film structures. JETP Lett. 2008;88(1):31–35. DOI: 10.1134/S0021364008130079.
45. Drozdovskii AV, Cherkasskii MA, Ustinov AB, Kovshikov NG, Kalinikos BA. Formation of envelope solitons of spin-wave packets propagating in thin-film magnon crystals. JETP Lett. 2010;91(1):16–20. DOI: 10.1134/S0021364010010042.
46. Sheshukova SE, Morozova MA, Beginin EN, Sharaevskii YP, Nikitov SA. Formation of gap solitons in a finite magnonic crystal. Phys. Wave Phen. 2013;21(4):304–309. DOI: 10.3103/S1541308X13040134.
47. Grishin SV, Moskalenko OI, Pavlov AN, Romanenko DV, Sadovnikov AV, Sharaevskii YP, Sysoev IV, Medvedeva TM, Seleznev EP, Nikitov SA. Space-quasiperiodic and time-chaotic

parametric patterns in a magnonic quasicrystal active ring resonator. Phys. Rev. Appl. 2021;16(5):054029. DOI: 10.1103/PhysRevApplied.16.054029.
48. Kivshar YS, Agrawal GP. Optical Solitons: From Fibers to Photonic Crystals. New York: Academic Press; 2003. 540 p. DOI: 10.1016/B978-0-12-410590-4.X5000-1.
49. Gurevich AG, Melkov GA. Magnetization Oscillations and Waves. Boca Raton: CRC Press; 1996. 464 p.
50. Mednikov AM. Nonlinear effects at surface spin wave propagation in the YIG films. Soviet Physics, Solid State. 1981;23(1):242–245 (in Russian).
51. Temiryazev AG. Mechanism of surface magnetostatic wave frequency conversion under three-magnon decay conditions. Soviet Physics, Solid State. 1987;29(2):313–319 (in Russian).
52. Melkov GA, Sholom SV. Parametric excitation of spin waves by a surface magnetostatic wave. Sov. Phys. JETP. 1989;69(2):403–407.
53. Vashkovskii AV, Stal'makhov VS, Sharaevskii YP. Magnetostatic Waves in Microwave Electronics. Saratov: Saratov University Publishing; 1993. 312 p. (in Russian).
54. Kozhevnikov AV, Dudko GM, Khivintsev YV, Sakharov VK, Vysotskii SL, Nikulin YV, Pavlov ES, Khitun AG, Filimonov YA. Magnetic field direction influence on the spectrum of spin waves output signals at three-magnon decay of magnetostatic surface waves in a cross based on waveguides of yttrium iron garnet film. Izvestiya VUZ. Applied Nonlinear Dynamics. 2020;28(2):168–185 (in Russian). DOI: 10.18500/0869-6632-2020-28-2-168-185.
55. Dewar G. Applicability of ferrimagnetic hosts to nanostructured negative index of refraction (left-handed) materials. In: Proc. SPIE. Vol. 4806. Complex Mediums III: Beyond Linear Isotropic Dielectrics, 24 June 2002, Seattle, WA, United States. Washington, US: SPIE; 2002. P. 156–166. DOI: 10.1117/12.472980.
56. Amel'chenko MD, Grishin SV, Sharaevskii YP. Fast and slow electromagnetic waves in a longitudinally magnetized thin-film ferromagnetic metamaterial. Tech. Phys. Lett. 2019;45(12):
1182–1186. DOI: 10.1134/S1063785019120022.
57. Sharaevskaya AY, Kalyabin DV, Beginin EN, Fetisov YK, Nikitov SA. Surface spin waves in coupled easy-axis antiferromagnetic films. J. Magn. Magn. Mater. 2019;475:778–781. DOI: 10.1016/j.jmmm.2018.11.130.
58. Belov PA, Marqués R, Maslovski SI, Nefedov IS, Silveirinha M, Simovski CR, Tretyakov SA. Strong spatial dispersion in wire media in the very large wavelength limit. Phys. Rev. B. 2003;67(11):113103. DOI: 10.1103/PhysRevB.67.113103.
59. High Frequency Magnetics Software [Electronic resource]. Devon, UK: MaxLLG, Innovation Centre, University of Exeter; 2019. Available from: https://www.maxllg.com.
60. Aziz MM. Sub-nanosecond electromagnetic-micromagnetic dynamic simulations using the finite-difference time-domain method. Progress In Electromagnetics Research B. 2009;15(15):1–29. DOI: 10.2528/PIERB09042304.
61. Sadovnikov AV, Rozhnev AG. Electrodynamical characteristicsof periodic ferromagnetic structures. Izvestiya VUZ. Applied Nonlinear Dynamics. 2012;20(1):143–159 (in Russian). DOI: 10.18500/0869-6632-2012-20-1-143-159.
62. Vansteenkiste A, Leliaert J, Dvornik M, Helsen M, Garcia-Sanchez F, Van Waeyenberge B. The design and verification of MuMax3. AIP Advances. 2014;4(10):107133. DOI: 10.1063/1.4899186.